

# A TMD-based model for Hadronization off heavy nuclei

F. A. Ceccopieri and R. Dupré\*

*Université Paris-Saclay, CNRS, IJCLab, 91405, Orsay, France*

(Dated: August 30, 2023)

## Abstract

Semi-inclusive deep inelastic scattering (SIDIS) off nuclei is a unique process to study the parton propagation mechanism and its modification induced by the presence of the nuclear medium. It allows us to probe the medium properties, particularly the cold nuclear matter transport coefficient, which can be directly linked to the nuclear gluon density. We present here a model for hadron production in deep inelastic lepton-nucleus scattering, which takes into account the hadronic transverse momentum of final state particles via transverse-momentum dependent (TMD) parton distributions and fragmentation functions. We implement parton energy loss and hadronic absorption with a geometrical model of the nucleus. The model is compared with the nuclear SIDIS multiplicity ratios and transverse-momentum broadening data from the CLAS, HERMES, and EMC collaborations, aiming for a simultaneous description of these data sets. We obtain a good agreement over the various nuclear targets and the wide kinematical range of those experiments. We best describe the data with a transport coefficient  $\hat{q} = 0.3 \text{ GeV/fm}^2$ , and we highlight the importance and the role of correlations in extracting this quantity.

Keywords: first keyword, second keyword, third keyword

---

\*Correspondence email address: raphael.dupre@ijclab.in2p3.fr

## I. INTRODUCTION

The fragmentation of quarks into hadrons, *i.e.* hadronization, is a complex dynamical process of QCD. It is extensively studied in the vacuum and can be described by perturbative QCD and non-perturbative fragmentation functions [1]. This process is modified in the presence of a medium, such that studying the modification of the hadron spectra allows the extraction of certain medium properties. Conversely, a medium with known properties can be used for the study of the space-time development of the hadronization process [2]. Such studies require careful consideration of the longitudinal and transverse components of the hadron spectra simultaneously. Here, we will study this problem using a model based on transverse momentum dependent (TMD) parton distribution functions (PDF) and fragmentation functions (FF). Recently, much progress has been made on TMD studies for proton, deuteron, and nuclei [3–5]. We present here a TMD model for hadron production in heavier nuclei and test it against the nuclear hadronization data sets from the EMC [6], HERMES [7–9] and CLAS [10] collaborations.

The present study includes two main nuclear effects: induced energy loss and nuclear absorption. The former is related to elastic collisions of the propagating parton, and the latter to the inelastic collision of the prehadron with nucleons. The interface of those two mechanisms is the production length,  $L_P$ , *i.e.* the length necessary for the quark to turn into a color-singlet prehadron. Energy loss and nuclear absorption are complementary, but there is no consensus in the literature on their respective quantitative contributions. The analysis presented in this paper aims at building a model which accommodates both effects and can describe an extensive data set with proper tuning of the production length  $L_P$  and the quark transport coefficient,  $\hat{q}$ . The latter is the key parameter of induced energy loss calculations, defined as the amount of transverse momentum the parton gains per unit of length of traversed material. The hadron production in semi-inclusive deep-inelastic scattering (SIDIS) off nuclei is the best observable for extracting these quantities.

Several groups have performed similar work in the past [11–13], often with a focus on energy loss [14–21] and transverse components only. Monte-Carlo event simulation is also sometimes used to approach the problem in a fully consistent way [22, 23] with the advantage of naturally including correlations. We aim to extend these previous works by using a TMD framework to describe the longitudinal and transverse components, as well as their

correlations.

## II. TMD CROSS SECTIONS

We consider the process

$$\ell(l) + N(P) \rightarrow \ell(l') + h(P_h) + X, \quad (1)$$

where  $\ell$  denotes the beam lepton,  $N$  the nucleon target,  $h$  the produced hadron and  $X$  the remainder of the hadronic final state. Particles four-momenta are given in parentheses. As customary, we define the photon momentum to be  $q = l - l'$ , and we introduce the invariants  $Q^2 = -q^2$ ,  $\nu = p \cdot q/M$ ,  $x_B = Q^2/2P \cdot q$ ,  $y = P \cdot q/P \cdot l$ ,  $W^2 = (P + q)^2$ , and  $z = P \cdot P_h/P \cdot q$ . We define  $P_{h\perp}$  to be the transverse components of hadron momentum  $P_h$  with respect to the virtual photon momentum, defined in the target rest frame, and  $\phi_h$  the angle between the leptonic and the hadronic planes following the Trento convention [24]. Throughout this paper, we work in the one-photon exchange approximation and neglect the lepton mass. However, we retain in the calculation, when necessary, the nucleon mass  $M$  and the hadron  $h$  mass,  $M_h$ . Here we consider only the positively-charged pion production for simplicity. We assume that polarization is not measured. The semi-inclusive lepton-hadron cross-section, summed over the helicities of the incoming lepton, and integrated over the azimuthal angle  $\phi_h$  of the outgoing hadron can be written as [25]

$$\frac{d^4\sigma}{dx_B dy dz dP_{h\perp}^2} = \frac{2\pi^2\alpha^2}{x_B^2 s} \frac{[1 + (1 - y)^2]}{y^2} F_{UU,T}, \quad (2)$$

where  $\alpha$  is the fine structure constant and the structure function on the r.h.s. depends on  $x_B$ ,  $Q^2$ ,  $z$  and  $P_{h\perp}^2$ . The first and second subscripts of the above structure functions indicate the respective polarization of the beam and the target, whereas the third subscript specifies the polarization of the virtual photon. As all our analysis is performed at the lowest order in the strong coupling, the contribution of the longitudinal structure function  $F_{UU,L}$  is absent at this order of accuracy. The structure function  $F_{UU,T}$  can be expressed as a convolution over partonic transverse momenta as

$$F_{UU,T} = x_B \sum_q e_q^2 \int d^2\mathbf{p}_\perp d^2\mathbf{k}_\perp \delta^{(2)}(\mathbf{p}_\perp + z\mathbf{k}_\perp - \mathbf{P}_{h\perp}) f_{q/P}(x_B, \mathbf{k}_\perp) D_{h/q}(z, \mathbf{p}_\perp), \quad (3)$$

where  $f_{q/P}(x_B, \mathbf{k}_\perp)$  and  $D_{h/q}(z, \mathbf{p}_\perp)$  represent the TMD unpolarised parton distribution in the proton and TMD unpolarised fragmentation functions into pions, respectively. Here  $\mathbf{k}_\perp$

represents the transverse momentum of the initial state parton with respect to the virtual photon direction and  $\mathbf{p}_\perp$  the transverse momentum of the detected hadron relative to the fragmenting parton. The delta function is a direct consequence of transverse momentum conservation. TMD PDFs and FFs are normalized to give the corresponding collinear distributions upon integration over transverse momentum. The summation runs over quarks and antiquarks at this order.

In the following, we will turn these expressions into a form suitable for phenomenological applications. Convolution integrals in Eq. 3 can be analytically performed under the hypothesis that the transverse momentum and the light-cone fraction dependencies of TMD densities could be factorized by assuming a Gaussian shape of the transverse part; such an assumption is known to be good at low transverse momentum. Therefore we use for the TMD PDFs and FFs the following ansatz:

$$f_{q/P}(x_B, \mathbf{k}_\perp) = f_{q/P}(x_B) \frac{1}{\pi \langle k_\perp^2 \rangle} e^{-k_\perp^2 / \langle k_\perp^2 \rangle} \quad (4)$$

and

$$D_{h/q}(z, \mathbf{p}_\perp) = D_{h/q}(z) \frac{1}{\pi \langle p_\perp^2 \rangle} e^{-p_\perp^2 / \langle p_\perp^2 \rangle}. \quad (5)$$

This simplified approach also allows us to include the transverse momentum broadening when considering SIDIS on nuclear targets in a relatively economical way, which is for us crucial given the cumbersome cross sections appearing in that case.

In such approximations, the structure function in Eq. 3 can be eventually rewritten as:

$$F_{UU,T} = x_B \sum_q e_q^2 f_{q/P}(x_B) D_{h/q}(z) \frac{e^{-P_{hT}^2 / \langle P_{hT}^2 \rangle}}{\pi \langle P_{hT}^2 \rangle} \quad (6)$$

where the additive nature of Gaussian convolution sets the average hadronic transverse momentum  $P_{hT}$  to

$$\langle P_{hT}^2 \rangle = \langle p_\perp^2 \rangle + z^2 \langle k_\perp^2 \rangle. \quad (7)$$

For the collinear unpolarized PDFs, we adopt **MSTW08** leading order set [26] whereas, for the collinear FFs, we adopt the leading order set **DSS** [27]. In the present analysis, we include the evolution of the above collinear functions, but we neglect the full TMD evolution, which would unnecessarily weigh down the formalism and would require additional modelization in the nuclear case [5].

We will integrate our model over the experimental bins thus creating some sensitivity to the shape of the  $z$  and  $p_\perp$  spectra on the proton target. To model these, we take inspiration

from the parametrization of Barone *et al.* [28], which preserves the kinematical structure induced by the convolution of the initial and final state Gaussians in Eq. 7 and model the widths as:

$$\langle p_{\perp}^2 \rangle(z) = (A + B z^2)(1 - z)^C, \quad (8)$$

$$\langle k_{\perp}^2 \rangle(z) = D. \quad (9)$$

In addition to the original ansatz of [28], following Ref. [29], we introduce here a large- $z$  dampening factor controlled by parameter  $C$ . The four parameters are determined using the width of pion  $P_{h\perp}$ -spectra in slices of  $z$  extracted via Gaussian fits to the HERMES proton and deuteron data [30] and the widths of  $P_{h\perp}$ -spectra on a deuteron target from HERMES [8]. The optimized parameters used in our simulation are  $A = 0.141 \text{ GeV}^2$ ,  $B = 1.195 \text{ GeV}^2$ ,  $C = 0.736$  and  $D = 0.065 \text{ GeV}^2$ .

Finally, realistic results are obtained only after the proper implementation of the kinematic cuts used in the data set we try to reproduce. In particular, the contribution of target fragmentation is not accounted for in our formalism. Therefore, we apply a cut on Feynman  $x$ , with  $x_F = 2h_z^*/W$ ,  $h_z^*$  being the hadron third component defined in the  $\gamma P$  center-of-mass frame, whenever specified by the kinematical selection of a given data set. Next, we consider the cut on the invariant mass of the system  $X$  ( $M_X$ ), where the latter represents the hadronic final state but with the measured final state hadron  $h$  excluded. In all our calculations, we enforce the condition  $M_X > M$ , which induces a sizeable decrease of the  $P_{h\perp}$ -width at large  $z$  and low  $\nu$ .

### III. NUCLEAR EFFECTS

The two main observables used by the experiments are the multiplicity ratios

$$R_h^A(\nu, Q^2, z, P_{hT}^2) = \frac{N_h^A(\nu, Q^2, z, P_{hT}^2)/N_e^A(\nu, Q^2)}{N_h^D(\nu, Q^2, z, P_{hT}^2)/N_e^D(\nu, Q^2)}, \quad (10)$$

and the transverse momentum broadening

$$\Delta p_T^2 = \langle P_{hT}^2 \rangle_A - \langle P_{hT}^2 \rangle_D, \quad (11)$$

where  $A$  stands for the atomic mass number,  $N_e$  and  $N_h$  the number of inclusive and semi-inclusive events, respectively, and the observables being both normalized to deuterium,  $D$ .

### A. Production length and nuclear medium density

We implement the nuclear effects under the hypothesis that energy loss takes place before absorption. Thus, we need to know the length of the total traversed material, and the production length  $L_P$ , where parton energy loss ends and absorption starts. To go further and account for the density profile of the nucleus, we need to define effective lengths. To do so, we assume that the incident photon scatters on a parton belonging to a nucleon at position  $x_i, \vec{b}_i$ , with the origin fixed to the nuclear center. The scattered parton then moves along the positive  $x$  direction. We describe the nuclear matter distribution with a Wood Saxon distribution,  $\rho(x, \vec{b}_i)$ , normalized to  $A$ . With this in mind, we adopt the following definition of total path length traversed in nuclear matter:

$$L_T^*(x_i, \vec{b}_i) = \frac{1}{\rho(0, 0)} \int_{x_i}^{\infty} dx \rho(x, \vec{b}_i). \quad (12)$$

The production length, *i.e.* the length traveled by the colored parton before forming a pre-hadron, is parametrized with a form already used in previous studies [2]:

$$L_P(z, \nu) = N z^\lambda (1 - z)^\beta \left( \frac{\nu}{\nu_0} \right)^\gamma, \quad (13)$$

where  $N$ ,  $\lambda$ ,  $\beta$ ,  $\nu_0$ , and  $\gamma$  are parameters that will be adjusted to data. In the present study, we do not explore the interesting possibility that  $L_P$  might depend on other variables, such as  $P_{hT}^2$  or  $Q^2$ . Similarly to the total path length  $L_T^*$ , we define an effective production length that accounts for the density as follows

$$L_P^*(z, \nu; x_i, \vec{b}_i) = \frac{1}{\rho(0, 0)} \int_{x_i}^{x_i + L_P(z, \nu)} dx \rho(x, \vec{b}_i). \quad (14)$$

### B. Partonic energy loss

When partons traverse a QCD medium such as the nucleus, we expect them to emit gluons and lose some of their energy along the way. Several groups have tackled the problem of calculating this energy loss with a rather large spread of results [31]. We chose to use the calculation by Arleo [32], based on the BDMPs calculations [33, 34]. In this framework, the energy loss  $\epsilon$  depends on the transport coefficient and the length of the medium through the characteristic gluon energy

$$w_c = \frac{1}{2} \hat{q} L_P^{*2}. \quad (15)$$

The energy loss probability distribution  $W(\epsilon)$  by Arleo includes also the dependence on the outgoing parton energy which we take to be  $\nu$ . It is expressed as follows:

$$\overline{W}(\bar{\epsilon}, \bar{\nu}) = \frac{1}{\sqrt{2\pi}\sigma(\bar{\nu})\bar{\epsilon}} \exp\left[-\frac{(\log \bar{\epsilon} - \mu(\bar{\nu}))^2}{2\sigma(\bar{\nu})^2}\right], \quad (16)$$

where barred variables are normalized to  $\omega_c$ , the functions  $\mu$  and  $\sigma$  are empirical [32] and its normalized version is defined by  $\overline{W}(\bar{\epsilon} = \epsilon/\omega_c) = \omega_c W(\epsilon)$ . We model nuclear-modified FFs according to the kinematic rescaling proposed by Wang, Huang and Sarcevic [35], which amounts to shift the argument of the collinear FFs:

$$z_* = \frac{z}{1 - \epsilon/\nu}. \quad (17)$$

The implementation of such a rescaling allows us to obtain the nuclear-modified TMD FFs:

$$zD_{q/A}(z, p_\perp, \langle p_\perp^2 \rangle(z); Q^2) = \int_0^{(1-z)\nu} d\epsilon W(\epsilon, \nu, \hat{q}, L_P^*) z_* D_{q/N}(z_*, p_\perp, \langle p_\perp^2 \rangle(z_*); Q^2), \quad (18)$$

which generalizes the collinear variables rescaling proposed in Ref. [35] to transverse ones. Moreover, we use the connection proposed by BDMPS to link the energy loss  $\epsilon$  to  $\langle q_\perp^2 \rangle$ , the average transverse momentum acquired by the parton traversing the medium [36, 37]:

$$-\frac{dE}{dx} = \mathcal{K} \frac{\alpha_s N_C}{4} \langle q_\perp^2 \rangle, \quad (19)$$

with  $E$  the energy of the gluon emitter,  $N_C$  the number of colors,  $\alpha_s$  the strong coupling constant and the factor  $\mathcal{K}$  for the unit change. From this, we can link the transverse momentum broadening to the parton energy loss:

$$\langle q_\perp^2 \rangle = \frac{4\epsilon}{\mathcal{K}\alpha_s N_C L_P^*}, \quad (20)$$

which is therefore distributed according to Eq.16. This source of final state transverse momentum, assuming it is distributed as a Gaussian, adds to the final state transverse momentum of the TMD FFs. However, since this transverse momentum is acquired in the same process as the energy loss it will be scaled by  $z_*$  instead of  $z$ .

### C. Absorption

After the production length, a prehadron starts to form and might interact with the medium, thus not giving rise to a measured hadron in the final state. To simulate this, we

use an attenuation factor of the form:

$$n_{att}(z, \nu; x_i, b_i) = 1 - \left[ \frac{L_T^* - L_P^*}{L_{typical}} \right]^d, \quad (21)$$

with  $L_{typical}$  and  $d$  free parameters. This simple phenomenological parametrization is constructed such as to introduce a correlation between the size of the medium and the absorption process, via the length traversed by the prehadron in the medium,  $L_T^* - L_P^*$ . At any fixed value of  $L_T^*$ , the attenuation is maximal for small  $L_P^*$  and it is vanishing for large  $L_P^*$ . This aims to describe the transition from one regime to the other without resorting to the unknown prehadron-nucleon cross-section. The attenuation factor  $n_{att}$  does implicitly depend on  $z$  and  $\nu$  through the dependence of  $L_P^*$  on those variables. We further assume that it is quark-flavor independent and apply it as a multiplicative factor in defining nuclear FFs in Eq. 18.

We do not attribute transverse momentum in association with the pre-hadron interaction as the elastic process contributes very little compared to inelastic processes [15]. Thus, we consider here that the pre-hadrons are absorbed in the nucleus and give rise to fragments in the target fragmentation region outside our model's domain.

#### D. Fermi motion

Among the initial state effects we need to consider is the Fermi motion of the nucleons in the nuclear targets. We use the parametrizations of 3-momentum distributions,  $n_A(\vec{P})$  presented in Ref. [38]. We neglect the effect of Fermi motion in the longitudinal direction due to its small size relative to the typical energies involved in the experiments we aim to describe. As we only consider the transverse contribution, we define the average transverse Fermi motion as

$$\langle P_T^2 \rangle_A = \frac{\int d^3\vec{P} P_T^2 n_A(\vec{P})}{\int d^3\vec{P} n_A(\vec{P})}, \quad (22)$$

where adopting spherical coordinates, the transverse momentum is defined with respect to the  $z$ -axis, corresponding to the incoming photon direction. Projecting out transverse components, the integral can be written as

$$\langle P_T^2 \rangle_A = \frac{2}{3} \int_0^\infty P^4 dP n_A(P). \quad (23)$$



The calculation returns an average transverse Fermi motion of around  $0.011 \text{ GeV}^2$  for deuterium which rises fast to  $0.036 \text{ GeV}^2$  for carbon, and then flattens out for heavier nuclei and ends around  $0.044 \text{ GeV}^2$  for a lead nucleus.

This source of initial state transverse momentum, assuming it is distributed as a Gaussian with widths provided by the calculation adds to the nucleon's initial state partonic transverse momentum. A  $z^2$  term will therefore weigh both of them.

### E. Nuclear structure functions

Putting together all the elements discussed above, the unpolarized nuclear structure function reads

$$F_{UU,T}^A = x_B \sum_q e_q^2 f_{q/A}(x_B, Q^2) \int dx_i \int d^2\vec{b}_i \frac{\rho(x_i, b_i)}{A} \int_0^{(1-z)\nu} d\epsilon \frac{W(\epsilon, \nu, \hat{q}, L_P^*)}{1 - \epsilon/\nu} n_{att}(z, \nu; x_i, b_i) D_{q/P}(z_*, Q^2) \frac{e^{-P_{hT}^2 / \langle P_{hT}^2 \rangle(z_*)}}{\pi \langle P_{hT}^2 \rangle(z_*)} \quad (24)$$

where  $f_{q/A}(x_B)$  are the nuclear PDFs, which we simulate as a linear combination of free proton and neutron PDFs, where the latter are obtained via isospin invariance. This basic approach is justified by our observables, which are not sensitive to the collinear nuclear effects on parton distributions. This simplification is allowed by the double ratio in Eq. 10, which cancels PDF contributions, and the transverse momentum broadening in Eq. 11, which is only sensitive to transverse dynamics.

We assume that all sources of transverse momentum broadening have a Gaussian distribution such that their convolution gives an overall Gaussian with a width

$$\langle P_{hT}^2 \rangle_A = \langle p_\perp^2 \rangle(z_*) + z^2 [\langle k_\perp^2 \rangle + \langle P_T^2 \rangle_A] + z_*^2 \langle q_\perp^2 \rangle. \quad (25)$$

The first term is the width of the fragmentation function but evaluated, according to Eq. (18), at  $z_*^2$ . The terms weighted by  $z^2$  are for the initial state parton momenta intrinsic in the nucleon and the nuclear Fermi motion. The last term accounts for the nuclear broadening due to parton energy loss and is weighted by  $z_*^2$ .

The observables introduced in Eq. (10) and Eq. (11) are both normalized to the deuterium. The model discussed so far is designed to describe heavy nuclei but shows sizeable nuclear effects when it is extrapolated to deuterium. Therefore, both observables are normalized to our modeled deuterium to ensure a proper normalization.

## IV. RESULTS

### A. Energy loss only parametrization

Among the two mechanisms we consider, the partonic energy loss has been extensively studied in the literature and has a solid theoretical background. Therefore, in a first attempt, we tried to describe the data with that mechanism alone, being responsible for both the depletion of hadron yields and the broadening of transverse momentum. Within this picture, absorption is switched off by letting  $L_P \rightarrow \infty$ , so that  $L_T^* = L_P^*$  and consequently  $n_{att} = 1$  in Eq. 21. Under this approximation, we present in the top panels of Fig. 1 the comparison of the HERMES multiplicity ratios as a function of  $z$  and  $P_{hT}^2$  with our default value  $\hat{q} = 0.3 \text{ GeV/fm}^2$ . The multiplicity ratios show a clear deficit in normalization (leftmost panels) while the  $p_t$ -broadening,  $\Delta\langle P_{hT}^2 \rangle$ , is fairly reproduced (rightmost panel). The normalization issue of the former can be alleviated by using a larger value of  $\hat{q} \sim 0.9 \text{ GeV/fm}^2$ , as shown in the bottom left panels of Fig. 1. However, such a large  $\hat{q}$  entering in Eq. 19, leads to an abnormally large  $p_t$ -broadening, by far greater than the one seen in the data (bottom right panel). The contradiction highlighted by those findings can be overcome by assuming that another mechanism is at work to reduce the yields, *i.e.* absorption. The attenuation is produced by inelastic interactions of the so-called prehadrons, a colorless state yet to become real hadron, with the medium, possibly creating secondary particles with lower energies. Under the hypothesis that elastic prehadron-nucleon cross sections are small, neither broadening nor energy loss is generated in such a phase.

### B. Full model parametrization

At this point, we include the *ad hoc* absorption from Eq. 21 for which we need to find suitable parameters. Our aim is not to make the best possible description of the data in all corners like in a fit. To adjust our parameters, we concentrate on kinematics which are the safest in terms of TMD factorization [39] ( $0.3 < z < 0.8$ ), parton energy loss applicability ( $\nu > 10$ ), and the Gaussian TMD model ( $P_{h\perp}^2 < 0.5 \text{ GeV}^2$ ). We will check later whether our model can be extrapolated out of this kinematic region, so we concentrate here on a subset of the HERMES data [8, 9] to tune our parameters.

We show in Fig. 2 and Fig. 3 a selection of data according to the criteria listed above

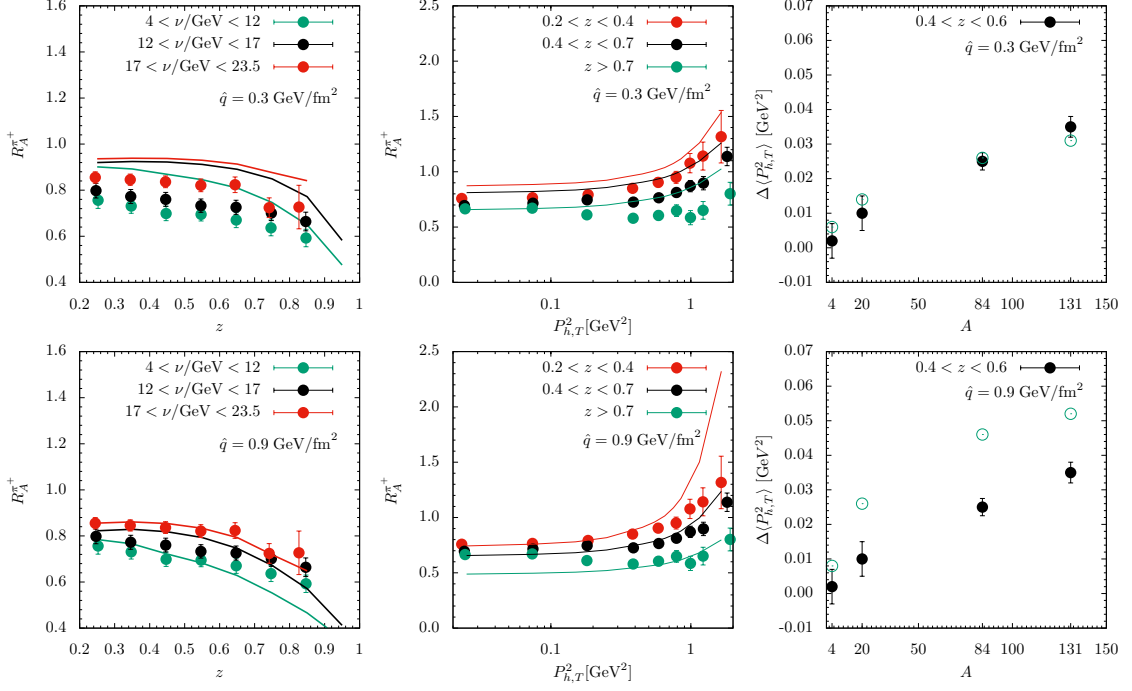


Figure 1:  $\pi^+$ -multiplicity ratio on a Krypton target, with absorption switched off, *i.e.*  $L_P \rightarrow \infty$ , with  $\hat{q} = 0.3 \text{ GeV/fm}^2$  (top panels) and  $\hat{q} = 0.9 \text{ GeV/fm}^2$  (bottom panels). We present the multiplicity ratios as a function of  $z$  (leftmost column) and as a function of  $P_{h,T}^2$  (middle column). In the rightmost column, we present the  $p_t$ -broadening,  $\Delta\langle P_{h,T}^2 \rangle$ , as a function of  $A$ . Data from the HERMES collaboration [8].

together with the model with adjusted parameters summarized in Tab. I. The overall agreement is satisfactory, but a few preliminary comments can be made immediately about the parameters obtained. We notice that the exponent parameters for the production length ( $\lambda$ ,  $\beta$  and  $\gamma$ ) are small compared to previous modelisations [2]. In particular, with  $\lambda = 0$  and  $\beta = 0.25$ , we significantly suppress the  $z$  dependence of  $L_P$  to describe the data adequately. This is needed to not over-suppress the hadron yield at both  $z$  extremes. We show in Tab. II the typical production lengths obtained with this set of parameters for the CLAS, HERMES, and EMC data. We observe that these results are consistent with previous work [2].

We obtain a transport coefficient value for cold nuclear matter,  $\hat{q} = 0.3 \text{ GeV/fm}^2$ , which is larger than some of the most recent extractions [20, 21]. However, these previous works neglect the correlation between longitudinal and transverse components. We attribute our different result to a survivor bias: because the measured transverse momentum broadening

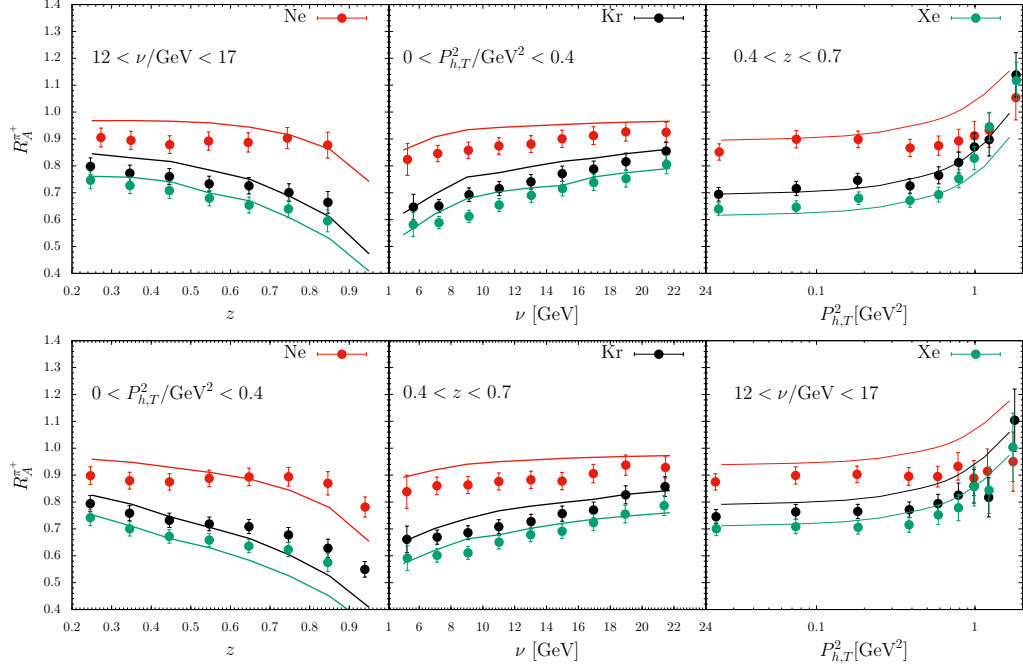


Figure 2: Multiplicity ratio for  $\pi^+$  on different nuclear targets as a function of various kinematical variables in selected ranges. Data from the HERMES collaboration [8].

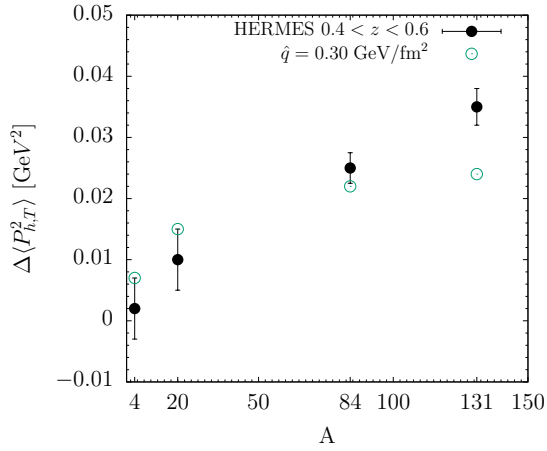


Figure 3:  $\pi^+$  transverse momentum broadening in the range  $0.4 < z < 0.6$  as a function of  $A$ . Data from the HERMES collaboration [8].

is obtained only through the detected hadrons, it is thus indirectly affected by absorption. In the HERMES data, the hadron yield is reduced by 20-30% in Krypton, whatever model is used it is clear that the suppressed part of the spectrum will be strongly correlated to the

Production length				
$N$	$\lambda$	$\beta$	$\gamma$	$\nu_0$
4.0 fm	0.0	0.25	0.3	1 GeV
Transport coefficient		Nuclear absorption		
$\hat{q}$	$\alpha_s$	$L_{typical}$	$d$	
0.3 GeV/fm <sup>2</sup>	0.5	2 fm	0.5	

Table I: From top to bottom: final parametrization of the production length, the transport coefficient, and the parameters controlling the nuclear absorption.

	$E_{beam}$	$\langle \nu \rangle$	$\langle z \rangle$	$L_P$
	[GeV]	[GeV]		[fm]
CLAS	5	3	0.5	4.7
HERMES	23.5	10	0.5	6.7
EMC	280	100	0.35	14.3

Table II: Values of  $L_P$  in the average kinematics of different experiments whose data are considered in this paper.

length of nuclear material traversed. So effectively, the transverse momentum observables select hadrons that have interacted less with the nuclear medium. Thus, it creates a correlation between absorption and energy loss that reduces the measured transverse momentum broadening and motivates to use a larger  $\hat{q}$ . This effect can already be observed in our first test with energy loss only in Fig. 1. There, it is clear that despite a factor 3 in  $\hat{q}$  between the two scenarios explored, the transverse momentum broadening increases by less than a factor 2 for krypton. Together, our results indicate that this effect is large no matter what the source of the hadron yield quenching is, and thus it needs to be accounted for in the description of the transverse momentum dependent observables.

With the hadron absorption parameters, we can notice that the coefficient  $d$  indicates the dependence on the path length. Our best value,  $d = 0.5$ , indicates that the pre-hadron absorption is reducing as it propagates. Such behavior is possible through a filtering effect

where compact prehadrons survive longer, and thus absorption effect drops. However, this is in direct contradiction with the results of previous studies [11, 13, 22]. The difference between the results presented in those studies and our approach are numerous, but they are likely linked to the way  $L_P$  is parameterized.

### C. Comparison to HERMES data

Going into more details on Fig. 3, we observe that the  $A$  dependence of  $\Delta p_T^2$  is not completely satisfactory, as the model overshoots the light nuclei and undershoots heavier nuclei. This problem is a common feature of numerous descriptions of this observable in the literature [15, 19–21]. The best description we obtain of this observable is in Fig. 1, where production length is set to infinity and absorption is thus completely deactivated. It appears impossible to resolve this issue with existing model frameworks because reducing the production length to increase the contribution of absorption further degrade the description of this observable. We conclude that all the models (ours included) are still missing an element contributing to the shape of the transverse momentum broadening as a function of the atomic number  $A$ .

We compare our model to more HERMES multiplicity ratio data in Fig. 4 and note that all displayed dependencies are pretty well reproduced. Some of the high  $z$  behaviors are missed. However, as discussed above, this is a phase space where TMDs do not dominate the cross-section. Thus, we do not expect our model to describe this phase properly. To further analyze the behavior of transverse momentum broadening, we compare our model to more HERMES data in Fig. 5. In the top left figure, our model reproduces the observed hadronic transverse momentum on deuterium. However, on the same figure, we observe that the transverse momentum broadening shape as a function of  $z$  appears to be largely off for all nuclear targets. At low  $z$ , this is to be expected as target fragmentation might contribute, but at large  $z$  it is more puzzling. Given the structure of Eq. 25, the rising pattern of  $\Delta\langle P_{hT}^2 \rangle$  against  $z$  is expected. Of the previously cited literature, only Domdey et al. [15] shows the same observable, reporting a similar discrepancy. Furthermore, we show in the same figure our model with and without Fermi motion. We observe that the latter is the main contribution at large  $z$ . The absence of such a basic effect is surprising. We suspect correlated errors in the data to be at the origin of this behavior as all nuclei are

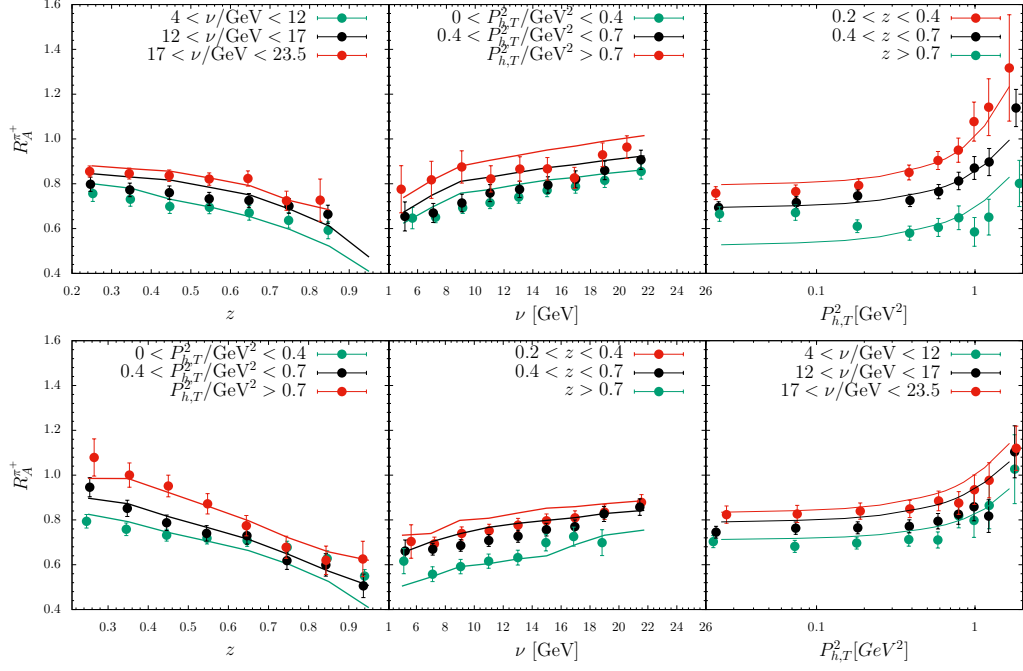


Figure 4: Multiplicity ratio for  $\pi^+$  on a Krypton target as a function of kinematic variables compared to our model with parameters as in Tab. [I]. Data from the HERMES collaboration [8].

normalized to the same deuterium data. Otherwise, that would indicate that factorization is largely broken in this kinematical region. To reduce the Fermi motion contribution to the broadening effect, it is also possible to normalize the observable to heavier nuclei like helium, carbon, or neon, for which Fermi motion contribution is much larger than deuterium.

#### D. Comparison to CLAS data

The critical test for the model and the parametrization of  $L_P$  is to check to which extent they can describe data in different energy ranges. So, we compare our model, with unchanged parameters, to the multiplicity ratio for positively-charged pions measured by the CLAS Collaboration [10]. The lower energy of the beam ( $E_e = 5.014$  GeV) implies a much lower range of lepton energy transfer variable  $\nu$ , compared to the HERMES case. The applicability of the TMD factorization and framework at such low energy on nuclei is clearly questionable, nevertheless we found, in general, a satisfactory agreement of our model with the data, but some features are worthwhile to be discussed.

In Fig. 6, we present the multi-dimensional multiplicity ratios as a function of  $z$  for three

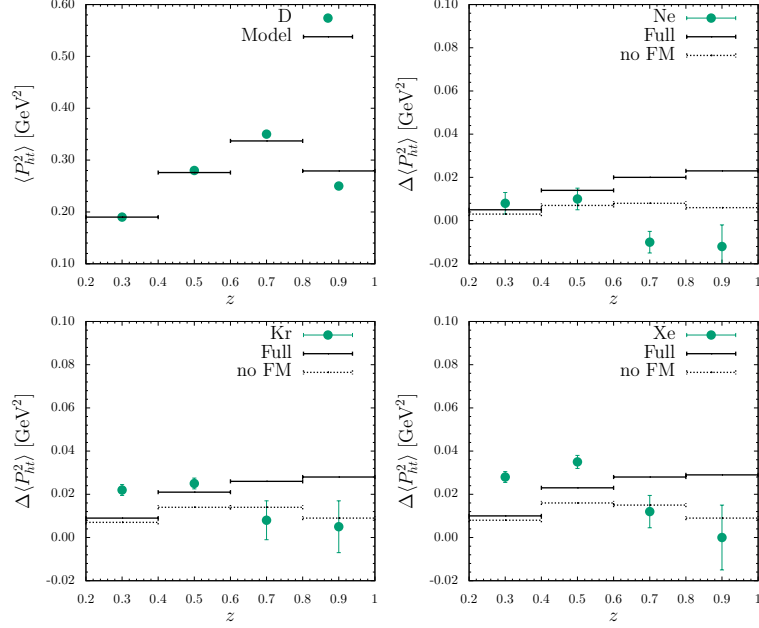


Figure 5:  $\pi^+$  widths on deuterium (top left panel) and transverse momentum broadening on various heavy nuclei as a function of  $z$  compared to HERMES data of Ref. [8]. Our model is shown with (solid lines) and without (dotted) Fermi motion contribution.

$\nu$  ranges and three target nuclei. For clarity, we did not show the different  $Q^2$  bins in this figure since the dependence on this variable is very weak. Our model also predicts tiny  $Q^2$  dependence in accord with the data. We reproduce very well the  $z$ -shapes, and the model slightly overshoots the multiplicity ratio for the light target (carbon) and slightly undershoots the one on the heavier (lead). The data does not show a dependence on  $\nu$  in contrast with HERMES results, a feature reproduced by our model in this energy range. In the same figure, we present our calculation with absorption switched off in dotted lines. The impact of absorption for this data set is maximal and essentially driven by the  $\nu$ -dependence of  $L_P$ . Comparing the two sets, one may see the increasing impact of absorption in going from light to heavier nuclei, a direct consequence of the correlation introduced by the absorption mechanism in Eq. 21.

In Fig. 7, we present the multiplicity ratios as a function of the hadronic  $P_{hT}$  in slices of  $z$  for different nuclear targets. Setting aside the visible normalization issue in some  $z$  bins outlined above, we notice two things. First, the slope of the multiplicity ratios as a function of  $P_{hT}$  is reducing as we go to higher  $z$ , which our model describes correctly at



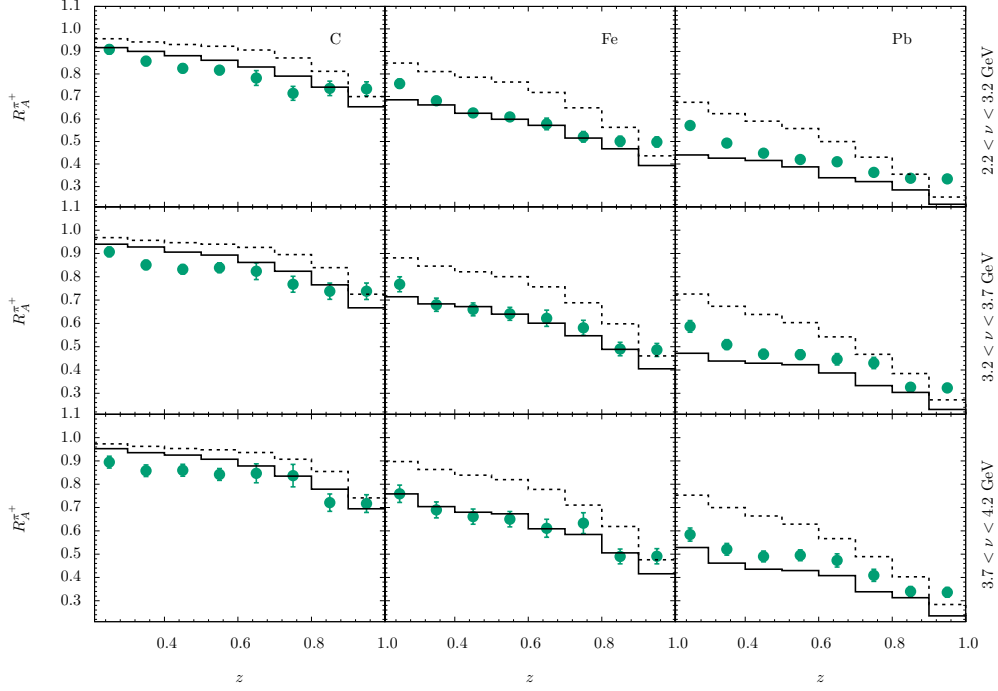


Figure 6:  $\pi^+$  multiplicity ratios as a function of  $z$  for three different nuclear targets integrated in bins of  $\nu$  and in  $1.3 < Q^2 < 1.8 \text{ GeV}^2$ . Our model is shown with default values (solid lines) and with absorption switched off, *i.e.*  $L_P \rightarrow \infty$  (dotted). Data from CLAS Collaboration [10].

small  $P_{hT}$ . Second, the slope increases significantly as  $P_{hT}$  increases, likely due to our pure Gaussian shape transverse momentum model. However, it could also be a sign that the model generates an amount of broadening smaller than the one in the data, particularly with this discrepancy getting more pronounced going from light to heavy nuclei. In the absence of transverse momentum broadening results from CLAS, it is difficult to conclude definitely on this aspect.

### E. Comparison to EMC data

We finally compare our model to the multiplicity ratios data from the EMC collaboration on a copper target [6]. The collected data refer to multiplicity ratios for the sum of charged hadrons, which we approximate as the sum of charged pions since the latter largely dominates the hadronic yields. This data set is particularly handy since it allows us to test our model in the transition region from intermediate values of  $\nu \sim 20 \text{ GeV}$  up to the asymptotic limit,

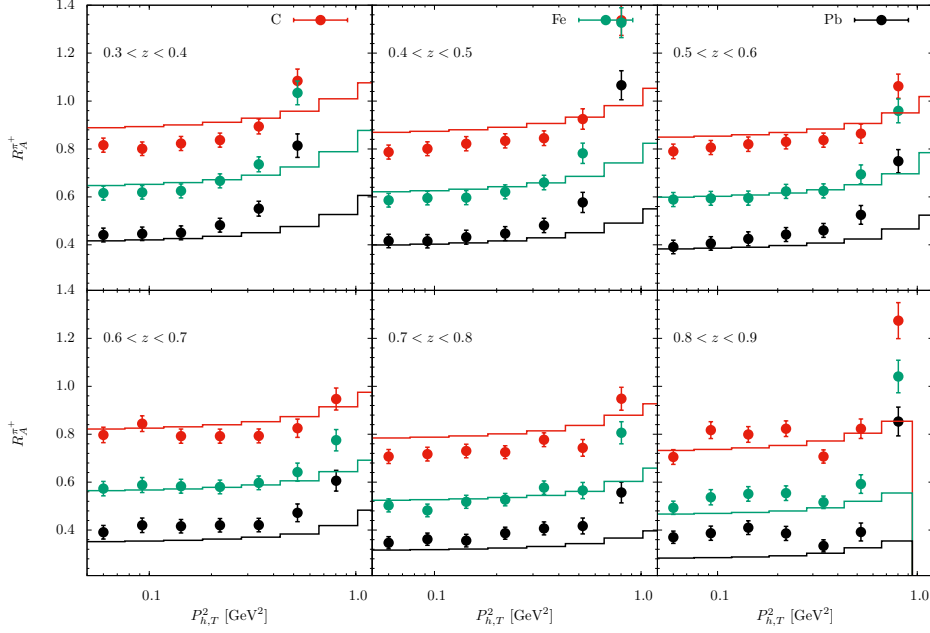


Figure 7:  $\pi^+$  multiplicity ratios as a function of  $P_{h,T}^2$  in various  $z$  bins for three different nuclear targets. Data from CLAS Collaboration [10].

where nuclear effects vanish.

In Fig. 8, we present our model compared to data. The overall description is very good, particularly the shape of multiplicity ratios as a function of  $z$  and  $\nu$ . We also present the calculation with absorption switched off (dotted lines): the comparison with the full model shows that, given the larger energy transfer, absorption has a much weaker impact on this data set. Nevertheless, absorption still gives a sizeable contribution at the lower  $\nu$  and is necessary to match the normalization and shape observed in the data. We conclude that the energy extrapolation is modeled correctly and reproduces the vanishing of nuclear effects.

## V. CONCLUSIONS

We applied a TMD-based model to describe the nuclear SIDIS data of the CLAS, HERMES, and EMC collaborations, with the aim of a simultaneous description of multiplicity ratios and transverse momentum broadening. We found that using a model with parton energy loss alone leads to inconsistencies in the combined description of those observables, which can be instead achieved by adding a pre-hadron absorption mechanism. After tuning

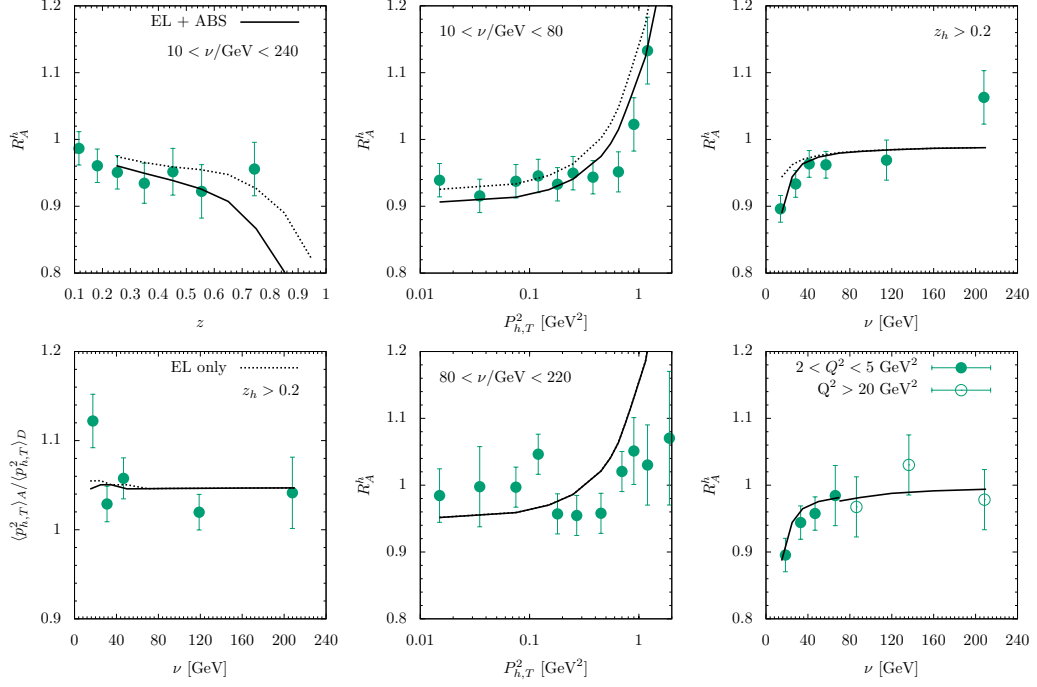


Figure 8: Charged hadrons multiplicity ratios on copper as a function of various kinematic variables, compared to data from the European Muon Collaboration [6]. Solid lines are for the model with energy loss (EL) plus absorption (ABS), while dashed ones are for the model with energy loss (EL) only. The bottom left panel shows the ratio of hadronic average transverse momentum on the nucleus over that on the deuterium.

the model parameters, we found a satisfactory agreement with all the data sets considered. We best describe the data with a cold nuclear matter transport coefficient value  $\hat{q} = 0.3 \text{ GeV/fm}^2$ , but this value is strongly correlated with the parametrization of both the absorption mechanism and the production length  $L_P$ .

We find strong correlations between the observables and, in particular, an important effect of survivor bias on the transverse momentum broadening measurement. This demonstrates the importance of simultaneously describing both observables to extract the transport coefficient, and more generally, to study the transverse effects in nuclei and understand hadronization off nuclei in SIDIS. The model describes the data on a very wide range of energies from  $\nu = 2 \text{ GeV}$  to  $\nu = 200 \text{ GeV}$ . We find that at low lepton energy transfer, hadron absorption is responsible for the majority of the depletion observed in multiplicity ratios, while at higher lepton energy transfer, parton energy loss becomes relatively more

important, until the smooth vanishing of all nuclear effects at the highest energies. The model finally presents problems in describing the correct  $A$  and  $z$  dependences of the transverse momentum broadening. This issue definitely requires further investigations on both the experimental and theoretical front to be resolved.

## VI. ACKNOWLEDGEMENTS

We acknowledge many fruitful discussions with A. Accardi, F. Arleo and S. Peigne. This work has received funding from the European Research Council (ERC) under the European Union’s Horizon 2020 research and innovation programme (Grant agreement No. 804480)

- 
- [1] R. L. Workman *et al.* (Particle Data Group), “Fragmentation Functions in  $e^+e^-$ ,  $ep$ , and  $pp$  Collisions,” in *Prog. Theor. Exp. Phys. 2022, 083C01* (2022) Chap. 19, p. 375.
  - [2] A. Accardi, F. Arleo, W. K. Brooks, D. D’Enterria, and V. Muccifora, *Riv. Nuovo Cim.* **32**, 439 (2010), arXiv:0907.3534 [nucl-th] .
  - [3] H. Avakian, A. Bressan, and M. Contalbrigo, *Eur. Phys. J. A* **52**, 150 (2016), [Erratum: *Eur.Phys.J.A* 52, 165 (2016)].
  - [4] A. Bacchetta, *Eur. Phys. J. A* **52**, 163 (2016), arXiv:2107.06772 [hep-ph] .
  - [5] M. Alrashed, D. Anderle, Z.-B. Kang, J. Terry, and H. Xing, *Phys. Rev. Lett.* **129**, 242001 (2022), arXiv:2107.12401 [hep-ph] .
  - [6] J. Ashman *et al.* (European Muon Collaboration), *Z. Phys. C* **52**, 1 (1991).
  - [7] A. Airapetian *et al.* (HERMES Collaboration), *Nucl.Phys.* **B780**, 1 (2007), arXiv:0704.3270 [hep-ex] .
  - [8] A. Airapetian *et al.* (HERMES), *Phys. Lett. B* **684**, 114 (2010), arXiv:0906.2478 [hep-ex] .
  - [9] A. Airapetian *et al.* (HERMES), *Eur. Phys. J. A* **47**, 113 (2011), arXiv:1107.3496 [hep-ex] .
  - [10] S. Moran *et al.* (CLAS), *Phys. Rev. C* **105**, 015201 (2022), arXiv:2109.09951 [nucl-ex] .
  - [11] B. Kopeliovich, J. Nemchik, E. Predazzi, and A. Hayashigaki, *Nucl.Phys.* **A740**, 211 (2004), arXiv:hep-ph/0311220 [hep-ph] .
  - [12] A. Accardi, D. Grunewald, V. Muccifora, and H. J. Pirner, *Nucl. Phys. A* **761**, 67 (2005), arXiv:hep-ph/0508036 .

- [13] B. Guiot and B. Z. Kopeliovich, Phys. Rev. C **102**, 045201 (2020), arXiv:2001.00974 [hep-ph] .
- [14] Z.-t. Liang, X.-N. Wang, and J. Zhou, Phys. Rev. D **77**, 125010 (2008), arXiv:0801.0434 [hep-ph] .
- [15] S. Domdey, D. Grunewald, B. Kopeliovich, and H. Pirner, Nucl.Phys. **A825**, 200 (2009), arXiv:0812.2838 [hep-ph] .
- [16] J.-H. Gao, Z.-t. Liang, and X.-N. Wang, Phys. Rev. C **81**, 065211 (2010), arXiv:1001.3146 [hep-ph] .
- [17] L.-H. Song and C.-G. Duan, Phys.Rev. **C81**, 035207 (2010).
- [18] Y.-k. Song, J.-h. Gao, Z.-t. Liang, and X.-N. Wang, Phys. Rev. D **89**, 014005 (2014), arXiv:1308.1159 [hep-ph] .
- [19] Y.-k. Song, Z.-t. Liang, and X.-N. Wang, Phys. Rev. D **89**, 117501 (2014), arXiv:1402.3042 [nucl-th] .
- [20] P. Ru, Z.-B. Kang, E. Wang, H. Xing, and B.-W. Zhang, Phys. Rev. D **103**, L031901 (2021), arXiv:1907.11808 [hep-ph] .
- [21] W. K. Brooks and J. A. López, Phys. Lett. B **816**, 136171 (2021), arXiv:2004.07236 [hep-ph] .
- [22] K. Gallmeister and U. Mosel, Nucl. Phys. A **801**, 68 (2008), arXiv:nucl-th/0701064 .
- [23] W. Ke, Y.-Y. Zhang, H. Xing, and X.-N. Wang, (2023), arXiv:2304.10779 [hep-ph] .
- [24] A. Bacchetta, U. D’Alesio, M. Diehl, and C. A. Miller, Phys. Rev. D **70**, 117504 (2004), arXiv:hep-ph/0410050 .
- [25] A. Bacchetta, M. Diehl, K. Goeke, A. Metz, P. J. Mulders, and M. Schlegel, JHEP **02**, 093 (2007), arXiv:hep-ph/0611265 .
- [26] A. D. Martin, W. J. Stirling, R. S. Thorne, and G. Watt, Eur. Phys. J. C **63**, 189 (2009), arXiv:0901.0002 [hep-ph] .
- [27] D. de Florian, R. Sassot, and M. Stratmann, Phys. Rev. D **75**, 114010 (2007), arXiv:hep-ph/0703242 .
- [28] V. Barone, M. Boglione, J. O. Gonzalez Hernandez, and S. Melis, Phys. Rev. D **91**, 074019 (2015), arXiv:1502.04214 [hep-ph] .
- [29] M. Soleymaninia and H. Khanpour, Phys. Rev. D **100**, 094033 (2019), arXiv:1907.12294 [hep-ph] .

- [30] A. Airapetian *et al.* (HERMES), Phys. Rev. D **87**, 074029 (2013), arXiv:1212.5407 [hep-ex] .
- [31] N. Armesto *et al.*, Phys. Rev. C **86**, 064904 (2012), arXiv:1106.1106 [hep-ph] .
- [32] F. Arleo, JHEP **11**, 044 (2002), arXiv:hep-ph/0210104 .
- [33] R. Baier, Y. L. Dokshitzer, A. H. Mueller, S. Peigne, and D. Schiff, Nucl. Phys. B **483**, 291 (1997), arXiv:hep-ph/9607355 .
- [34] R. Baier, Y. L. Dokshitzer, A. H. Mueller, and D. Schiff, JHEP **0109**, 033 (2001), arXiv:hep-ph/0106347 [hep-ph] .
- [35] X.-N. Wang, Z. Huang, and I. Sarcevic, Phys. Rev. Lett. **77**, 231 (1996), arXiv:hep-ph/9605213 .
- [36] R. Baier, Y. L. Dokshitzer, A. H. Mueller, S. Peigne, and D. Schiff, Nucl. Phys. B **484**, 265 (1997), arXiv:hep-ph/9608322 .
- [37] R. Baier, Y. L. Dokshitzer, A. H. Mueller, and D. Schiff, Nucl.Phys. **B531**, 403 (1998), arXiv:hep-ph/9804212 [hep-ph] .
- [38] C. Ciofi degli Atti and S. Simula, Phys. Rev. C **53**, 1689 (1996), arXiv:nucl-th/9507024 .
- [39] M. Boglione, M. Diefenthaler, S. Dolan, L. Gamberg, W. Melnitchouk, D. Pitonyak, A. Prokudin, N. Sato, and Z. Scalyer (Jefferson Lab Angular Momentum (JAM)), JHEP **04**, 084 (2022), arXiv:2201.12197 [hep-ph] .